

Learning Brain Effective Connectivity Network Structure Using Ant Colony Optimization Combining With Voxel Activation Information

Jinduo Liu , Junzhong Ji , Xiuqin Jia , and Aidong Zhang , *Fellow, IEEE*

Abstract—Learning brain effective connectivity (EC) networks from functional magnetic resonance imaging (fMRI) data has become a new hot topic in the neuroinformatics field. However, how to accurately and efficiently learn brain EC networks is still a challenging problem. In this paper, we propose a new algorithm to learn the brain EC network structure using ant colony optimization (ACO) algorithm combining with voxel activation information, named as VACOEC. First, VACOEC uses the voxel activation information to measure the independence between each pair of brain regions and effectively restricts the space of candidate solutions, which makes many unnecessary searches of ants be avoided. Then, by combining the global score increase of a solution with the voxel activation information, a new heuristic function is designed to guide the process of ACO to search for the optimal solution. The experimental results on simulated datasets show that the proposed method can accurately and efficiently identify the directions of the brain EC networks. Moreover, the experimental results on real-world data show that patients with Alzheimers disease (AD) exhibit decreased effective connectivity not only in the intra-network within the default mode network (DMN) and salience network (SN), but also in the inter-network between DMN and SN, compared with normal control (NC) subjects. The experimental results demonstrate that VACOEC is promising for practical applications in the neuroimaging studies of geriatric subjects and neurological patients.

Index Terms—Brain network, effective connectivity, bayesian network, ant colony optimization, voxel activation information.

I. INTRODUCTION

BRAIN effective connectivity (EC), defined as the neural influence that one brain region exerts over another [1], is important for the assessment of normal brain function, and its impairment is associated with neurodegenerative diseases such as Alzheimer's disease (AD) [2]–[5], Parkinson's disease (PD) [6]–[8], and Schizophrenia [9], [10]. Therefore, how to accurately and efficiently learn brain EC network from neuroimaging data, e.g., functional magnetic resonance imaging (fMRI), is becoming a hot study in neuroinformatics, where a great many of computational methods and mathematical models have been proposed for identifying the EC network related to human brain [11]–[21]. Naturally, learning brain effective connectivity can be considered as a problem of searching or constructing a directed graph structure from neuroimaging data. In other words, a brain EC network can be represented as a directed graph in which nodes denote brain regions, and the directed arcs denote effective connectivity between brain regions.

Generally the EC learning methods can be categorized into two types: the model-driven method and the data-driven method. The model-driven approach has been applied extensively for inferring the brain EC network, but this kind of methods requires prior assumptions on the models and is commonly used to construct the relatively small-scale networks [22]. So the data-driven approach, that can extract neural influences without the need of any prior assumptions or knowledge from fMRI data, gradually becomes the mainstream method in detecting the effective connectivity. Though data-driven methods have their own characteristics and are applicable to different fMRI data environments, they have some limitations on causal estimation [21]–[23]. For instance, Linear non-gaussian acyclic model (LiNGAM) method [14], [15] uses temporal independent component analysis (ICA) to infer effective connectivity from data, however, ICA requires a large number of datapoints, which make it perform poorly when the fMRI data sample is small [22]. Granger causality (GC) methods [16], [17] infer effective connectivity by the multiple regressions and require the fMRI time series to be wide-sense stationary, which may become

Manuscript received April 1, 2019; revised July 30, 2019, September 3, 2019, and October 4, 2019; accepted October 4, 2019. Date of publication October 10, 2019; date of current version July 2, 2020. This work was supported in part by the NSFC Research Program under Grant 61672065, in part (data collection and sharing) by the Alzheimer's Disease Neuroimaging Initiative (ADNI) under National Institutes of Health Grant U01 AG024904, and in part by DOD ADNI under the Department of Defense Award W81XWH-12-2-0012. (*Corresponding author: Junzhong Ji.*)

J. Liu and J. Ji are with the Beijing Municipal Key Laboratory of Multimedia and Intelligent Software Technology, College of Computer, Science and Technology, Faculty of information Technology, Beijing University of Technology, Beijing 100124, China (e-mail: liujinduo0607@emails.bjut.edu.cn; jjz01@bjut.edu.cn).

X. Jia is with the Department of Radiology, Xuanwu Hospital of Capital Medical University, Beijing 100053, China (e-mail: xqjia2014@163.com).

A. Zhang is with the Department of Computer Science and Biomedical Engineering, University of Virginia, Charlottesville, VA 22904 USA (e-mail: aidong@virginia.edu).

Digital Object Identifier 10.1109/JBHI.2019.2946676

unreliable when the underlying dynamics is dominated by unstable modes [21]–[23]. Generalized synchronization (GS) based method models the functional relation between the dynamics of coupled chaotic systems in the nonlinear dynamics [18]. GS employs some related measures to estimate the effective connectivity, e.g., non-linear interdependence measures (S index and H index) and normalized non-linear interdependence measure (N index) [11]. However, each of them has its own limitations. For instance, S index is not very robust against noise and signal length; H index is more robust against noise and easier to interpret than S index, but with the drawback that it is not normalized; N index is normalized but it reaches its maximum value of 1, only when the conditioned mean squared Euclidean distance is zero, which does not happen even if two brain regions are identically synchronized [20].

Recently, Bayesian network (BN) methods that are based on probability, statistics, and graph theory have gradually become an important and useful data-driven approach for identifying the brain EC network [24]–[26]. This is mainly because this kind of methods can accurately identify connections between brain regions [22]. However, BN methods perform well in identifying the connections, but they are rarely able to reliably and completely identify causal directions just as many other data-driven methods [22]. When the number of brain regions increases, the search space will become larger which results in the long running time and low direction identification ability of BN methods [24]–[26]. Besides, most of these methods only consider the distribution and statistical properties of fMRI data, and ignore some specific information (e.g., activation information, temporal information) of fMRI data [24]–[26]. Therefore, how to employ useful information from fMRI data to better infer effective connectivity is still an open and challenging research topic.

In this paper, we propose a novel method to learn the brain EC network structure using ant colony optimization (ACO) algorithm combining with voxel activation information, i.e., VACOEC. The main contributions of this paper, compared with our preliminary model [26], are as follows:

- We present a new strategy which uses the voxel activation information to measure the independence between each pair of brain regions and restrict the space of candidate solutions. The strategy can help the ACO avoid many unnecessary searches, and improve the time performance of the algorithm remarkably.
- We develop a new heuristic function of ACO by using the voxel activation information. The new heuristic function can instruct the ants to select the arcs which are more reasonable during the searching process, and improve the accuracy of the algorithm.
- We compare VACOEC with other state-of-the-art methods on simulated fMRI datasets, the results show that VACOEC has a stronger direction identification ability when learning brain effective connectivity network from fMRI data.
- We apply the new algorithm to two real fMRI datasets of AD, Mild Cognitive Impairment (MCI) and normal control (NC) subjects. The results show that some changes of effective connectivity in brain regions are related to

MCI and AD, which can help to explain and predict the progression and evolution of the AD disease.

II. RELATED WORK

A. Ant Colony Optimization for Learning Bayesian Networks (ACO-B)

ACO-B algorithm is a score-and-search approach for learning Bayesian networks by using K2 scoring metric to guide ants search for the global optimal solution (directed acyclic graph, DAG) [26], [27]. A brain effective connectivity network can be represented as a DAG $G = \langle \mathbf{V}, \mathbf{E} \rangle$, where \mathbf{V} is a set of nodes with each node $a \in \mathbf{V}$ representing a brain region; and \mathbf{E} is a set of arcs with each arc $\text{arc}_{ab} \in \mathbf{E}$ describing an effective connectivity between brain regions a and b . Thus learning brain EC network can be seen as a process of learning Bayesian network structure from fMRI data.

In ACO-B, each ant k begins with an empty graph $G(0)$ and incrementally constructs a solution by adding an arc at a time. The specific process of searching a BN by ACO algorithm is described below. The probabilistic transition rule of an ant k to select a arc arc_{ab} from the current candidate arcs at time t is defined as

$$\text{arc}_{ab} = \begin{cases} \arg \max_{a,b \in DA_k(t)} \{ [\tau_{ab}(t)] \cdot [\eta_{ab}(t)]^\beta \}, & \text{if } q \leq q_0 \\ \text{arc}_{a'b'}, & \text{otherwise} \end{cases}, \quad (1)$$

where $\tau_{ab}(t)$ and $\eta_{ab}(t)$ respectively represent the pheromone intensity and the heuristic information of the directed arc arc_{ab} ; β is the weighted coefficient which controls $\eta_{ab}(t)$ to influence the selection of arcs; $DA_k(t)$ ($a, b \in DA_k(t)$) is the set of all candidate arcs whose heuristic information is larger than zero; q_0 ($0 \leq q_0 < 1$) is an initial parameter that determines the relative importance of exploitation versus exploration (exploitation means selecting arcs by pheromone intensity and heuristic information, and exploration means global random selecting arcs); q is a random number which uniformly distributed in $[0, 1]$; and a pair of brain regions a' and b' are randomly selected according to the probability p :

$$p_{ab}^k(t) = \begin{cases} \frac{[\tau_{ab}(t)]^\alpha \cdot [\eta_{ab}(t)]^\beta}{\sum_{r,l \in DA_k(t)} [\tau_{rl}(t)]^\alpha \cdot [\eta_{rl}(t)]^\beta}, & \text{if } a, b \in DA_k(t) \\ 0, & \text{otherwise} \end{cases}, \quad (2)$$

where parameter α describes the relative importance of the pheromone $\tau_{ab}(t)$ left by the real ants. As the goal of ACO algorithm is to get the optimal structure whose K2 scoring metric is the maximum, the heuristic function of a directed arc is defined as:

$$\eta_{ab}(t) = f(a, Pa(a) \cup b) - f(a, Pa(b)), \quad (3)$$

for $\tau_{ab}(t)$, ACO-B respectively carries out two pheromone updating processes including local and global updating.

The algorithm will get the current optimal solution G^+ , when the iterations of ant colony are ended.

Because ACO-B algorithm adopts a stochastic search mechanism based on ACO, its quality is usually higher than that

of solutions obtained by many deterministic search methods. Besides, ACO algorithm can support information fusion easily, as it can integrate useful information in search process to help search.

B. Patel's Voxel Activation Model

The joint activation model of brain voxels is defined conceptually by Patel *et al.* [13]. In this model, Patel *et al.* developed two measurements of association (κ and τ) to describe the functional connectivity and effective connectivity based on the voxels activation probabilities. This method performs well relative to other methods on identifying brain effective connectivity, which has attracted some scholars' attention.

Smith *et al.* implemented Patel's method by recalculating each time series into the range [0, 1]. By comparing this method with other methods, they found that the direction identification ability of this method was better than all other algorithms [22].

Xue *et al.* developed a multimodal approach based on the joint activation in pairs of brain regions for network analysis [28]. They extended the measure of the activation in Patel's model, which evaluates joint activation only based on Cohens Kappa to describe functional connectivity (FC) and EC between pairs of brain regions. Then they further illustrated the advantages of the method by comparisons to methods that only incorporate functional information.

Although these methods have many advantages, there are some defects to limit their usage. 1) The connections obtained by Patel's κ are usually more than the actual connections, which results in low precision [22]. 2) The selection of the threshold is not very flexible, especially in the cases when ground truths are not available.

Therefore, how to further employ the useful information of the voxel activation model to more reasonably identify brain effective connectivity is a meaningful and challenging work. Thus, we subsequently try to combine the voxel activation information with the ACO-B algorithm to explore a new method for identifying the brain EC networks.

III. THE VACOEC ALGORITHM

In this section, we introduce the new method (VACOEC) for learning brain EC network structure from fMRI data.

A. Main Idea

To effectively learn a brain effective connectivity network, VACOEC employs two new strategies by using ACO with voxel activation information. The first strategy uses the voxel activation information to reduce the search space (called R. S.) while the second one employs a new heuristic function reinforced by the voxel activation information in ACO algorithm to heuristically guide search for an effective connectivity network (called new H. F.). Fig. 1 shows the flowchart of the VACOEC algorithm. First, we get the voxel activation information from fMRI data by calculating the joint and marginal activation probabilities for each pair of brain regions, e.g., the brain region *a* and the brain region *b*. Next, we use voxel activation information to

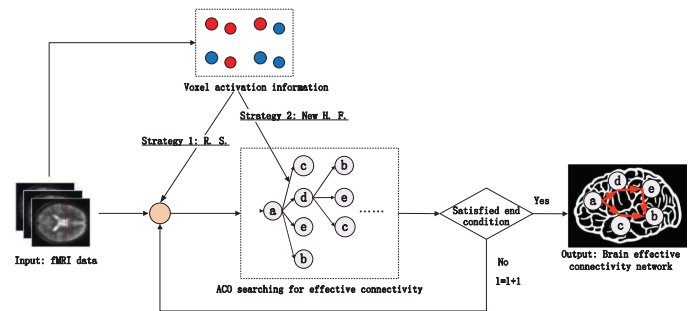


Fig. 1. The flowchart of the VACOEC algorithm.

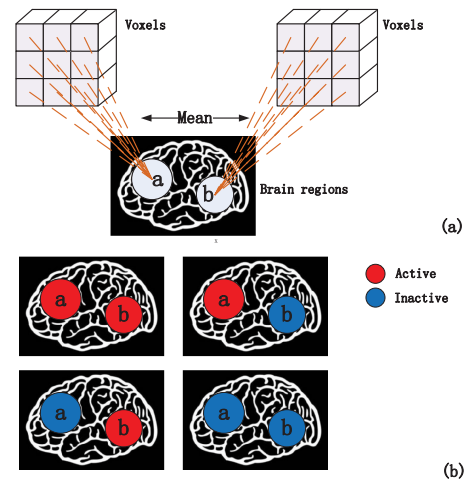


Fig. 2. Illustration of voxel joint activation: (a) The relationship between voxels and brain regions: a brain region is represented by the mean level of the all voxels in this area; (b) The four cases of the joint activation: 1) both region *a* and region *b* are active, 2) region *a* is active while region *b* is inactive, 3) region *a* is inactive while region *b* is active, and 4) both region *a* and region *b* are inactive.

determine whether there is a connection between brain regions *a* and *b*. After all connections of brain regions are determined, the candidate constraint network (CN) will be derived. Meanwhile, we propose a new heuristic function by using the voxel activation information to guide the ants searching for an optimal solution. Then the ants search for the brain effective connectivity network based on the candidate constraint network and the new heuristic function, and updates the pheromone to guide the next generation ants to search. Finally, when the search phase ends, the algorithm will get the brain EC network.

B. The Voxel Activation Information

In this paper, the representative voxel in a brain region is obtained by calculating the global mean of all voxels in this region. Fig. 2(a) shows the mapping between voxels and brain regions. Thus, a brain region is represented by the mean voxel, the voxel activation is also shown as the brain region activation.

For each fMRI time series in a brain region, we define

$$A = I(R_a > p), \quad (4)$$

TABLE I
THE JOINT ACTIVATION PROBABILITIES FOR BRAIN REGIONS a AND b

		Brain region a		
		Active	Inactive	
Brain region b	Active	θ_1	θ_3	$\theta_1 + \theta_3$
	Inactive	θ_2	θ_4	$\theta_1 + \theta_2$

where R_a is the timeseries of the representative voxel in region a , p is a threshold to measure whether a voxel is active, which is represented as $c \times \sigma$ in [13], and $I(\cdot)$ is the indicator function. Thus, A serves as an indicator of elevated regional brain activity, where the m^{th} element is 1 if the corresponding element of R_a is larger than p ; and the m^{th} element of A is 0 otherwise.

For each pair of regions a and b , the joint activation of this pair of brain regions can be interpreted as the four different cases, which are shown in Fig. 2(b). Then the joint activation probabilities for the corresponding four cases of brain regions a and b are shown in Table I.

In Table I, the four elements of θ_1 , θ_2 , θ_3 , and θ_4 are the joint activation probabilities corresponding to the above four cases, and $\theta_1 + \theta_2$ and $\theta_1 + \theta_3$ are the marginal activation probabilities for brain regions a and b , respectively. In detail, the joint activation probabilities θ_i ($i = 1, 2, 3, 4$) are defined as:

$$\begin{aligned}
 \theta_1 &= P(A_{asm} = 1, A_{bsm} = 1), \\
 \theta_2 &= P(A_{asm} = 1, A_{bsm} = 0), \\
 \theta_3 &= P(A_{asm} = 0, A_{bsm} = 1), \\
 \theta_4 &= P(A_{asm} = 0, A_{bsm} = 0).
 \end{aligned} \quad (5)$$

where s denotes s^{th} subject and m denotes m^{th} measurement. $A_{asm} = 1$ means that the brain region a of the s^{th} subject's m^{th} measurement is active, and it is inactive otherwise. A_{bsm} is similar to A_{asm} .

Then, we give the definition of voxel activation information:

Definition 3.1: The voxel activation information is a general term for the activation probability between voxel pairs, which contains the joint activation probabilities ($\theta_1, \theta_2, \theta_3$, and θ_4) and the marginal activation probabilities ($\theta_1 + \theta_2$ and $\theta_1 + \theta_3$).

C. Reducing Search Space Using Voxel Activation Information

From the original timeseries \mathbf{x}_a and \mathbf{x}_b of two brain regions a and b , first we linearly map them, and get the “normalised” timeseries \mathbf{n}_a and \mathbf{n}_b of a and b . The mapping method is described as follows: 1) Setting these values under the 10th percentile to 0, values over the 90th percentile to 1; and 2) Linearly mapping the other values to the range of [0, 1]. Next, we set a threshold p to define whether voxels in this pair of brain regions are active. If a voxel's value is higher than the threshold p , we set its value to 1, otherwise set its value to 0, then we will get the binary column vector \mathbf{v}_a and \mathbf{v}_b . Finally, we present a formula to calculate the joint activation probabilities θ_i in the following.

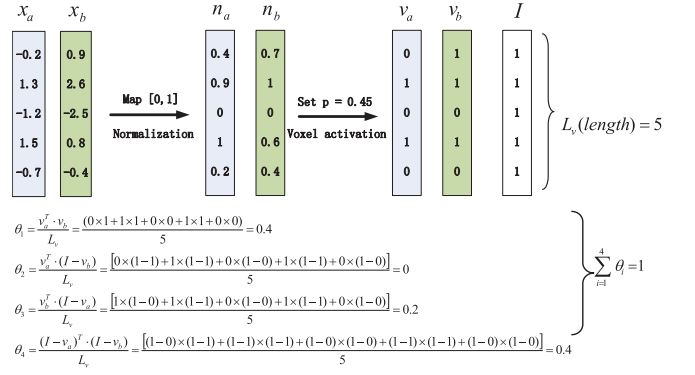


Fig. 3. An example of calculating the joint activation probabilities θ .

For $i = 1 \dots 4$, θ_i of two brain regions a and b can be calculated as:

$$\begin{aligned}
 \theta_1 &= \frac{\mathbf{v}_a^T \cdot \mathbf{v}_b}{L_v}, \\
 \theta_2 &= \frac{\mathbf{v}_a^T \cdot (\mathbf{I} - \mathbf{v}_b)}{L_v}, \\
 \theta_3 &= \frac{\mathbf{v}_b^T \cdot (\mathbf{I} - \mathbf{v}_a)}{L_v}, \\
 \theta_4 &= \frac{(\mathbf{I} - \mathbf{v}_a)^T \cdot (\mathbf{I} - \mathbf{v}_b)}{L_v},
 \end{aligned} \quad (6)$$

where L_v is the length of the voxel time series, \mathbf{I} is a column vector whose values are all 1 and has the same length with \mathbf{v}_a and \mathbf{v}_b . In order to more clearly illustrate this, we give an example to express this process in Fig. 3.

Based on the voxel activation information, we give two definitions in the following:

Definition 3.2: The synchronism of brain region activation is the set of states that two brain regions are activating at the same time.

Definition 3.3: The asynchronism of brain region activation is the set of states that one brain region is activating and the other brain region is inactivating.

From the definitions, we can find that the numerator of θ_1 is the measurement of the synchronism of brain region activation, and the θ_2 and θ_3 are the measurements of the asynchronism of brain region activation. Some synchronization research methods [11] have shown that stronger synchronization between two brain regions indicates that they are more likely to have connections.

Finally, a measure of association is employed to describe constraint network. The κ_{ab} of brain regions a and b is calculated as follows:

$$\kappa_{ab} = \frac{\theta_1 - E}{D(\max(\theta_1) - E) + (1 - D)(E - \min(\theta_1))}, \quad (7)$$

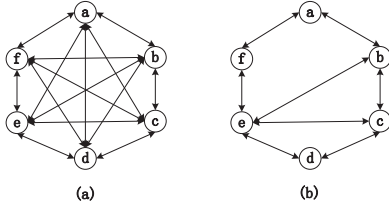


Fig. 4. The initial candidate connection graph: (a) the complete connection graph; (b) the possible connection graph.

where $E = (\theta_1 + \theta_2) \times (\theta_1 + \theta_3)$, $\max(\theta_1) = \min(\theta_1 + \theta_2, \theta_1 + \theta_3)$, $\min(\theta_1) = \max(0, 2\theta_1 + \theta_2 + \theta_3 - 1)$, and:

$$D = \begin{cases} \frac{\theta_1 - E}{2(\max(\theta_1) - E)} + 0.5, & \text{if } \theta_1 \geq E \\ 0.5 - \frac{\theta_1 - E}{2(E - \min(\theta_1))}, & \text{otherwise} \end{cases}, \quad (8)$$

The numerator of κ measures the difference between the joint probability and the expected joint probability of brain regions under the case of independence, and the denominator is simply a weighted normalizing constant forcing to range from -1 to 1 . $\max(\theta_1)$ represents the maximum value of join activation probabilities, while $\min(\theta_1)$ represents the minimum value of join activation probabilities. Consequently, according to Eq. (8), κ equals 1 when θ_2 or θ_3 equals 0 , and κ equals -1 when θ_1 or θ_4 equals 0 . The value of κ_{ab} that is close to 1 indicates a high degree of connectivity between two brain regions a and b . In other words, if two brain regions have strong synchronism, θ_1 is large, then the κ will be large, which indicates a stronger dependence relationship between these two brain regions. Conversely, the value of κ_{ab} will be 0 when the brain regions a and b are statistically independent.

Previous studies show that using some constraint knowledge from data to restrict the space of candidate solutions can effectively improve the efficiency of the algorithms for learning Bayesian networks from data [29], [30]. In detail, the deletion of redundant arcs greatly restricts the searching scope of the algorithms, reduces some sightless searching, and avoids many unnecessary constructing and scoring processes for those network structures including these redundant arcs. For a brain effective connectivity network, if κ_{ab} , for each pair of brain regions a and b , is larger than the threshold K we set, there will be a connection between them. A constraint network (CN), which consists of all connections with $\kappa_{ab} > K$, will be determined. Then the CN becomes the new search space of the algorithm, and the redundant arcs ($\kappa_{ab} < K$) will be prevented when constructing a solution.

For example, the initial connect graph is a complete connection graph which is shown in Fig. 4(a). Then we employ the voxel activation information to calculate the κ of all nodes, we find that κ_{ae} , κ_{ad} , κ_{ac} , κ_{bf} , κ_{bd} and κ_{cf} are less than the threshold K . So we delete these redundant arcs and get the possible connection graph which is shown in Fig. 4(b). Comparing the two different initial connect graphs with 6 nodes in Fig. 4, Fig. 4(a) is a complete connect graph with 6 nodes including 30 directed arcs and Fig. 4(b) is the possible connect graph only including

16 directed arcs through using the constraint knowledge. Due to many redundant arcs are deleted during the construct of a solution, the search space is greatly reduced.

D. A New Heuristic Function With the Voxel Activation Information

In ACO-B algorithm, if the arc $a \rightarrow b$ and arc $b \rightarrow a$ have the same K2 score, the ants will randomly select the node a or b to begin searching. The ants' random and blind searching may cause some reverse arcs in the final solution, and then reduce the search ability of the algorithm.

Considering the voxel activation information, we put forward a weighted factor ω as:

$$\omega = 1 + \frac{\theta_1 + \theta_2}{\theta_1 + \theta_3}, \quad (9)$$

where $\theta_1 + \theta_2$ and $\theta_1 + \theta_3$ are the marginal activation probabilities of two brain regions which reflect the activation relationships between this pair of brain regions. The denominator $\theta_1 + \theta_3$ is always larger than 0 . Since if θ_1 and θ_3 are close to 0 , according to Eq. (8), κ will be zero, and this arc will be deleted in the possible network structures.

As for two brain regions a and b , the marginal activation probability $\theta_1 + \theta_2$ shows the condition that brain region a is active while b is active or inactive, and the marginal activation probability $\theta_1 + \theta_3$ shows the condition that brain region b is active while a is active or inactive. Consequently, the ratio of $\theta_1 + \theta_2$ and $\theta_1 + \theta_3$ can objectively reflect the ascendancy of the corresponding two brain regions. In detail, $\theta_1 + \theta_2 > \theta_1 + \theta_3$ means the activation of brain region a is gaining ascendancy, which indicates arc $a \rightarrow b$ is more appropriate than arc $b \rightarrow a$. On the contrary, when $\theta_1 + \theta_2 < \theta_1 + \theta_3$, the activation of brain region b is gaining ascendancy, which shows arc $b \rightarrow a$ is more appropriate than arc $a \rightarrow b$. In other words, the new weighted factor has considered the characteristics of the activation of the brain regions, which contributes to guiding the ant to choose the more reasonable arcs, and then reduce the randomness and blindness of the searching.

Combining the limitation of the constraint candidate network with the weighted factor, the new heuristic function of an arc arc_{ab} is defined as:

$$\eta_{ab}(t) = \begin{cases} \omega \cdot (f(G_{h+1} : \text{Data}) - f(G_h : \text{Data})), & \text{if } \text{arc}_{ab} \in \text{CN} \\ 0, & \text{otherwise} \end{cases}, \quad (10)$$

where arc_{ab} is an arc from brain region a to brain region b and CN is the constraint network. From the formula, we can see that the constraint network can restrict the search scope and the weighted factor ω can guide an ant to select arcs. In other words, if an arc arc_{ab} is not in the constraint network, an ant will never select this arc, and the higher ω makes an ant more likely to select this arc.

Algorithm 1: VACOEC.

Input: fMRI Data.
Output: Brain effective connectivity network.

- 1 **Initialization:**
- 2 Set parameters $p, K, \alpha, \beta, q_0, \rho, w, Maxl$;
- 3 **Reducing search space:**
- 4 **for** every pair of brain regions (nodes) a and b **do**
- 5 Calculate the $\theta_1, \theta_2, \theta_3$ and θ_4 according to Eq.(7);
- 6 Calculate the κ_{ab} according to Eq.(8);
- 7 **end**
- 8 Obtain the constraint network (CN) by κ and K ;
- 9 **Searching for effective connectivity network:**
- 10 Set $G^+ = G(0), \tau_0 = 1/n \times |f(G(0) : Data)|$;
- 11 **repeat**
- 12 **for** $k = 1$ to w **do**
- 13 Ant k construct Graph (G_k);
- 14 set a random number $q[0, 1]$ and compare it with q_0 ;
- 15 add an arc arc_{ab} ($arc_{ab} \in CN$);
- 16 calculate the $K2$ metric of the G_k as $f(G_k : Data)$;
- 17 update η_{ab} according to Eq.(11);
- 18 update τ_{ab} ;
- 19 **if** ($f(G_k^{t+1} : Data) \leq f(G_k^t : Data)$) **then**
- 20 **break**;
- 21 **end**
- 22 **end**
- 23 $G_{(l)}^+ = \arg \max_k f(G_k : Data)$;
- 24 **if** ($f(G_{(l)}^+ : Data) \geq f(G_k : Data)$) **then**
- 25 $G^+ = G_{(l)}^+$
- 26 **end**
- 27 Perform global pheromone updating;
- 28 **until** ($G_{(l)}^+ = G_{(l-Maxl)}^+$);
- 29 **Return:** Effective connectivity network (G^+).

E. Algorithm Description and Complexity Analysis

The VACOEC algorithm mainly consists of two phases, i.e., reducing search space (using the voxel activation information) and searching for the effective connectivity network (based on a new heuristic with the voxel activation information), which is summarized in Algorithm 1.

The procedure of the proposed algorithm is to carry out initialization, reducing search space, searching for effective connectivity network, and return the effective connectivity network. After the initialization, the algorithm starts with the stage of reducing search space, where the joint active probabilities for every pair of brain regions are calculated according to the fMRI data. Then the algorithm calculates the κ for each pair of brain regions, and set threshold to get the constraint network (CN). In the stage of searching for an effective connectivity network, each ant search for an optimal solution instructed by the new heuristic information function and the pheromone. During each iteration, each ant adds an arc as a new component of a solution at a time, if the arc is not in the CN , it will never be added. The

algorithm obtains an optimal solution in the current iteration, when adding an arc can not make the $K2$ score of the solution higher. Then the algorithm updates the global pheromone to guide ants in the next generation going on searching. Once the algorithm obtains the same optimal solution for $Maxl$ successive generations, the search phase will end. After that, the algorithm gets the optimal solution which has the highest $K2$ value (G^+). Finally, VACOEC returns G^+ as the learned EC network.

Based on the description of Algorithm 1, the complexity of VACOEC can be simply analyzed as follows: Let the number of brain regions be N in a brain effective connectivity network. In the initialization process, the computing complexity is $O(1)$. In the reducing search space process, the time complexity is $O(N \cdot N) = O(N^2)$. For the process of searching for effective connectivity network, the time complexity is reduced from $O(l \cdot w \cdot N^2)$ to $O(l \cdot w \cdot x \cdot y)$ by using the constraint network, where l is the number of iterations, w is the number of ants, and $x \cdot y$ is the size of the constraint network. When the number of brain regions is very large, $x \cdot y$ will be significantly smaller than N^2 , thus the time performance of the VACOEC will be obviously enhanced.

IV. EXPERIMENTAL RESULTS AND DISCUSSION

To study the performance of VACOEC, we first employ some simulation fMRI datasets [22] to test the effects of parameters of the VACOEC algorithm. Then, we conduct a series of experiments on all Smith's simulation fMRI datasets to compare the proposed algorithm with other state-of-the-art algorithms. Finally, we use the real fMRI data which are obtained from Xuanwu Hospital of Capital Medical University and ADNI database to further validate and demonstrate the effectiveness of the VACOEC algorithm. The experimental platform is a PC with Intel Core i7-4770, 24 GB RAM, 2.40 GHz CPU, and Windows 7.

A. The Simulated fMRI Datasets

The simulated datasets contain 28 simulation cases which were created with different percent of noise and number of nodes [22]. The number of nodes in the 28 simulation cases is 5, 10, 15 or 50, respectively. In these simulation cases, the blood oxygen level dependent (BOLD) time series data are concatenated over 50 subjects and analyzed for each simulation dataset. The detail specifications for the 28 simulation datasets. Data were obtained from the <http://www.fmrib.ox.ac.uk/datasets/netsim/index.html> are shown in Table II. Particularly, the brain regions in the 28 simulated datasets are generated by dynamic causal models (DCM) [22], thus they do not represent for real brain regions, but can be viewed as a set of functional nodes (only measured by one global mean voxel).

B. Data Preprocessing

Like many other Bayes network algorithms, VACOEC employs the $K2$ score which cannot directly use the continuous

TABLE II
DESCRIPTION OF THE 28 SIMULATION CASES [22]

Sim	Nodes	Session (min)	TR (s)	Noise (%)	HRF (s)	Other factors
1	5	10	3.00	1.0	0.5	
2	10	10	3.00	1.0	0.5	
3	15	10	3.00	1.0	0.5	
4	50	10	3.00	1.0	0.5	
5	5	60	3.00	1.0	0.5	
6	10	60	3.00	1.0	0.5	
7	5	250	3.00	1.0	0.5	
8	5	10	3.00	1.0	0.5	shared inputs
9	5	250	3.00	1.0	0.5	shared inputs
10	5	10	3.00	1.0	0.5	global mean confound
11	10	10	3.00	1.0	0.5	bad ROIs (timeseries mixed with each other)
12	10	10	3.00	1.0	0.5	bad ROIs (new random timeseries mixed in)
13	5	10	3.00	1.0	0.5	backwards connections
14	5	10	3.00	1.0	0.5	cyclic connections
15	5	10	3.00	0.1	0.5	stronger connections
16	5	10	3.00	1.0	0.5	more connections
17	10	10	3.00	0.1	0.5	
18	5	10	3.00	1.0	0.0	
19	5	10	0.25	0.1	0.5	neural lag=100 ms
20	5	10	0.25	0.1	0.0	neural lag=100 ms
21	5	10	3.00	1.0	0.5	2-group test
22	5	10	3.00	0.1	0.5	nonstationary connection strengths
23	5	10	3.00	0.1	0.5	stationary connection strengths
24	5	10	3.00	0.1	0.5	only one strong external input
25	5	5	3.00	1.0	0.5	
26	5	2.5	3.00	1.0	0.5	
27	5	2.5	3.00	0.1	0.5	
28	5	5	3.00	0.1	0.5	

value of variables [25], [26]. Thus discrete processing is essential at the beginning. The discrete processing according to the number of time points, the discretized instance data are obtained for the whole brain, where each instance includes the discretized values of all brain regions (nodes) at the corresponding time point. For each node's timeseries of a subject, the range of voxel values is divided into several equal parts, and each part contains the same number of voxel values. Based on the division of node values, the voxel value of each node is quantized at every instance into a discrete value. For example, a node's time series is quantized into five parts, including very low (set value = 0), low (set value = 1), medium (set value = 2), high (set value = 3), and very high (set value = 4), with each of the five parts containing 20% of the data points.

C. Evaluation Metrics

In this section, we employ a set of measurements including Precision, Recall, and F-measure to evaluate the direction identification ability of algorithms.

Let GN express the ground-truth network and LN denote the learned network. The Precision, Recall and F-measure of directions are defined as follows:

$$\text{Precision}_d = \frac{D_s}{D_w + D_a + D_s}, \quad (11)$$

$$\text{Recall}_d = \frac{D_s}{TD}, \quad (12)$$

$$F_d = \frac{2 * \text{Precision}_d * \text{Recall}_d}{\text{Precision}_d + \text{Recall}_d}, \quad (13)$$

where D_s , D_w , D_a are employed to represent the direction differences between GN and LN. Specifically, D_s represents the

number of same arcs in GN and LN, D_a shows the number of extra added arcs in LN, D_w represents the number of arcs in LN whose connections are the same as those of GN and directions are different from the corresponding ones in GN, and TD is the total number of the directions in GN.

As is mentioned in [25], F-measure is a harmonic mean of Precision and Recall, so we only show the results of F_d to measure the network direction identification ability of algorithms on the 28 simulation cases for the sake of brevity.

D. Parameter Analyzing and Setting

To compare with other methods in a fair and appropriate way in the next section, we follow the parameter settings methods of the other comparison methods that we take some simulated fMRI datasets as examples to study the effects of the algorithm parameters [22], [25]. These parameters include the weights for the pheromone trail (α) and for the heuristic information (β), the controls of the pheromone evaporation (ρ), the relative importance of the exploitation versus exploration (q_0), the number of ants (n), the threshold of the voxels activation (p) and the threshold of the constraint networks (K). After a large number of experimental tests, we find that the set of parameters $\alpha = 1$, $\beta = 2$, $\rho = 0.2$, $q_0 = 0.8$, $n = 10$ performed well on most of datasets, and the parameters p and K are mainly associated with the number of nodes. Thus we test on the simulated data from Sim1 to Sim4 (number of nodes from 5 to 50) to determine a better parameter configuration of p and K for VACOEC. During all experiments, we employ the control variate technique that the value of a single parameter is changed, while keeping the values of other parameters fixed.

To objectively reflect the experimental results, we run 100 times and show the average results. We first set the default value of p and K as 0.6 and 0.2, and test the running time of VACOEC for different values of p and K . In Fig. 5, we give the form of box plots, where the top and the bottom of each box indicate the 75th and 25th percentiles, respectively; the line in each box indicates the 50th percentile; the whisker bars below and above each box indicate the minimum and maximum, respectively; and the squares and asterisks in each box indicate the mean and outliers, respectively. From Fig. 5(a)–(h) we can see that the decrease of p and the increase of K make the running time shorter. In particular, when K reaches 0.4, all paths will be constrained, and the algorithm cannot be executed.

Then we test how the solution quality (F_d) is influenced by p and K . In Fig. 6, we plot the effects of parameters on F_d from Sim1 to Sim4. From Fig. 6(a), we found that the value of p at 0.15, 0.3, 0.45 and 0.9 always performed worse or equal to p at 0.6 and 0.75, and then, as reflected in Fig. 6(b), the value of K at 0.1, 0.15, 0.25, 0.3 and 0.35 always performed worse or equal to K at 0.2. Considering both running time and solution accuracy (F_d), we finally set the p value at 0.6 and the K value at 0.2 in the following experiments.

E. Comparative Evaluations on the Simulated fMRI Data

To intuitively show the competitiveness of the VACOEC algorithm, we compare VACOEC algorithm with other seven

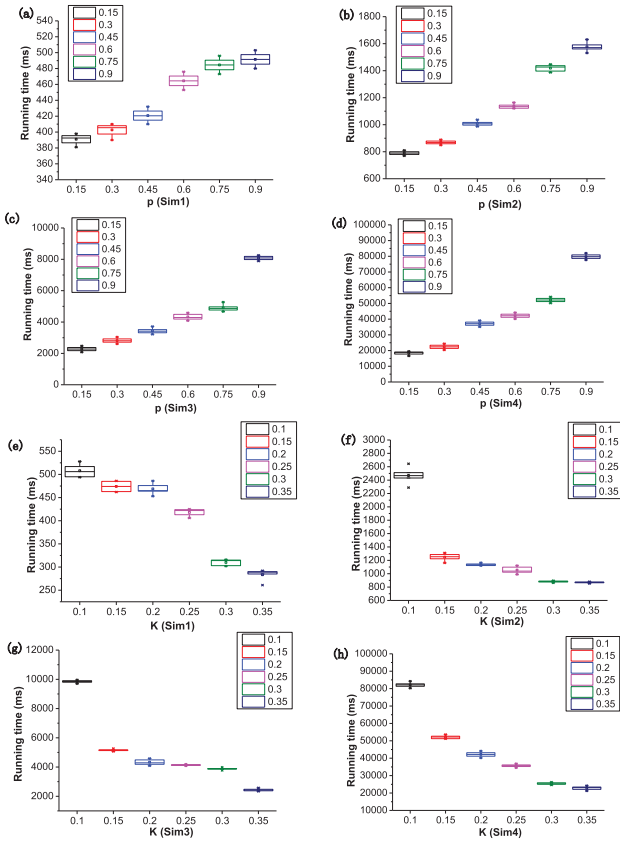


Fig. 5. The effects of the parameter p and K on time performance: (a, b, c, d) gives the box plots of running time (ms) for different values p from Sim1 to Sim4 when $K = 0.2$; (e, f, g, h) shows the box plots of running time (ms) for different values K from Sim1 to Sim4 as the $p = 0.6$.

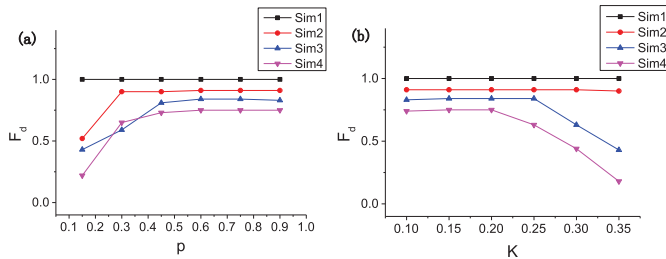


Fig. 6. The effects of parameter p and K on the F_d from Sim1 to Sim4: (a) gives how the F_d changes when the p increases ($K = 0.2$); (b) shows the plots of F_d for different values K ($p = 0.6$).

methods, some of them perform well on Smith's simulated dataset [22], and some of them are state-of-the-art methods. They are Prediction correlation (P-corr) method [19], LiNGAM method, GC method, GS method, Patel's condition dependence measurement method (Patel) [13], learning effective connectivity network using artificial immune algorithm (AIAEC) [25], and ACOEC [26], respectively. In particular, ACOEC is the preliminary algorithm that only using ACO to search for the brain effective connectivity (without considering voxel activation information), which is used to demonstrate the effectiveness of voxel activation information. The parameters of

TABLE III
The F_d VALUE OF 8 ALGORITHMS ON 28 SIMULATIONS

Sim	Algorithms							
	P-corr	LiNGAM	GC	GS	Patel	AIAEC	ACOEC	VACOEC
Sim1	0.80	0.91	1	0.60	0.80	1	1	1
Sim2	0.75	0.87	0.64	0.82	0.82	0.91	0.89	0.92
Sim3	0.56	0.84	0.65	0.89	0.84	0.84	0.86	0.87
Sim4	0.56	0.68	0.58	0.79	0.77	0.75	0.80	0.82
Sim5	1	1	0.60	1	1	1	1	1
Sim6	0.75	1	0.64	0.91	0.91	0.93	0.93	0.94
Sim7	1	1	0.80	1	1	1	1	1
Sim8	0.40	0.80	0.36	0.50	0.67	0.76	0.75	0.96
Sim9	0.80	0.80	0.55	0.62	0.83	0.84	0.82	0.85
Sim10	0.60	0.91	1	1	0.80	1	1	1
Sim11	0.62	0.61	0.54	0.64	0.74	0.59	0.59	0.61
Sim12	0.82	0.82	0.91	0.82	0.91	0.89	0.89	0.91
Sim13	0.63	0.40	0.22	0.25	0.50	0.64	0.64	0.64
Sim14	0.60	0.80	0.73	1	0.55	0.52	0.52	0.54
Sim15	0.20	0.55	0.46	0.46	0.83	0.96	0.96	0.96
Sim16	0.67	0.67	0.40	0.67	0.93	0.60	0.60	0.65
Sim17	0.82	0.91	0.72	1	0.91	0.98	0.98	0.98
Sim18	0.90	1	0.80	1	0.80	0.88	0.88	0.90
Sim19	0.80	1	0.67	1	0.80	1	1	1
Sim20	0.80	1	0.71	1	0.80	1	1	1
Sim21(a)	0.80	1	0.89	0.60	0.80	0.88	0.92	0.92
Sim21(b)	0.80	1	0.80	0.60	0.80	1	0.88	0.89
Sim22	0.40	0.17	0.44	1	1	1	1	1
Sim23	0.40	0.36	0.46	0.83	0.62	0.67	0.67	0.68
Sim24	0.20	0.50	0.57	0.43	0.62	0.68	0.68	0.69
Sim25	0.80	0.73	0.60	0.80	0.80	0.98	0.98	0.98
Sim26	0.20	0.60	0.33	0.60	0.80	0.96	0.96	0.98
Sim27	0.40	1	0.31	0.80	0.80	1	1	1
Sim28	0.80	1	0.67	1	0.80	1	1	1
Ave.	0.65	0.79	0.62	0.78	0.80	0.87	0.87	0.89

the algorithms under comparison are selected according to the existed literature and have been validating optimized by the previous works [19], [22], [25]. The default parameter configurations of the corresponding methods are as follows. P-corr runs with $BOLDMaxlength = 15, TR = 3$. LiNGAM uses the parameters where $Prune Factor = 1.0$. GC is set as $max_lag \in [1, 30], Alpha = 0.05$. GS is performed with $m = 10, nn = 10$, and $theiler = 50$. Patel runs with $bin = 0.75$. The AIAEC is set as $P_s = 0.5, P_c = 0.6, P_m = 0.4, T = 150, N = 80$, and $M = 70$. ACOEC uses the parameters where $\alpha = 1, \beta = 2, \rho = 0.2, q_0 = 0.8$. The VACOEC algorithm parameters are set as follows: $p = 0.6, K = 0.2, \alpha = 1, \beta = 2, \rho = 0.2, q_0 = 0.8, n = 10$. For each method, we show the results of the mean values (F_d and running time) over 100 runs on each simulation, which can reflect the ability of different methods for learning brain effective connectivity networks [22], [25]. To more intuitively see the performance of all algorithms, we also give the average results (Ave.) of each algorithm on all 28 simulated datasets.

The detailed comparison results of F_d value for all algorithms on 28 simulations are shown in Table III.

1) The factor of node number and session duration: From Sim1 to Sim4 in Table III, the number of nodes increases from 5 to 10, 15, and 50. Following the chain of Sim1-Sim2-Sim3-Sim4, we can see that most of the algorithms including VACOEC have a little decrease of F_d . Compared with AIAEC and ACOEC, VACOEC has a better and more stable performance as the number of nodes increases. In detail, when the number of nodes increases to 50, VACOEC's F_d value reach 0.82, which is higher than that of the other seven algorithms. Following the chain of Sim26-Sim25-Sim1-Sim5-Sim7, as the session duration

increase from 2.5 min, to 5 min, 10 min, 60 min, and 250 min. we can find that VACOEC can get the stable solution of the EC network from a short time to a long time, while other algorithms have an obvious setback when the session duration is short. In a word, a larger number of nodes and shorter session duration will affect the performance of most of the algorithms, however, VACOEC can still achieve a good performance.

2) Other impact factors: In Smith's simulated datasets, some other factors were given to test the algorithms on detecting the effective connectivity. In Sim8 and Sim9, external inputs are mixed into the network, which can be viewed as neuronal "noise". From the results in Table III, we can see that the external inputs seriously affect the performance of VACOEC and other algorithms. However, from the comparison results, we found VACOEC still has obvious advantages and the F_d value is higher than all of other algorithms. Sim10 has global mean confound, which means to add the same random time series to all node's BOLD time series. VACOEC performs well in this simulation which shows this factor has no affect to it. Sim11 and Sim12 show the factor of bad region of interests (ROIs). From the results in Table III, we find that bad ROIs in Sim11 seriously affect VACOEC and other algorithms, while Sim12 does not. In particular, VACOEC performs better than AIAEC and ACOEC in these two simulations. Sim13 shows the factor of backward connection, this factor obvious affect algorithms, and most of algorithms including VACOEC perform worse in this case. In Sim14, the ground-truth is a cyclic graph. This case is a problem for many of the global network modeling methods including most of the Bayesian network methods, due to it breaks the general modeling assumption in these methods, i.e., the graph has no cycle. From the results, we can see AIAEC, ACOEC and VACOEC perform worse, all falsely identifying the cyclic arc. So not accurately identifying cyclic connections is a limitation of Bayesian network method. In Sim15, the connection strength is increased from 0.4 to 0.9, which has a bad influences on most algorithms, but VACOEC performs quite well. In Sim16, the number of connections increases to seven from five, in this case, VACOEC performs better than GC, AIACE, and ACOEC but worse than P-corr, LiNGAM, GS and Patel. Sim18, Sim19, and Sim20 show the factor of low TR and HRF variability, VACOEC performs well and has a stable performance. Sim22 and Sim23 show the factor of nonstationarity and stationarity of connection strength between nodes. Most of the algorithms perform well in Sim22 while they perform worse in Sim23. These results indicate that nonstationary connection strength has less effect on detecting effective connectivity, while the stationarity connection has a bad effect for most of the algorithms. Sim25, Sim26, Sim27, Sim28 show the factor of different noises. From the results in Table III, we can find that VACOEC performs better than ACOEC in almost all simulations, which further demonstrate the effectiveness of the new strategies of VACOEC. Besides, VACOEC achieves the highest Ave., which indicates that VACOEC has a stronger direction identification ability compared with other algorithms. Therefore, we draw the conclusion that VACOEC performs well on almost all cases, especially at the situations when the session is short and the noise is significant.

TABLE IV
THE POST-HOC TEST RESULTS (P-VALUES) OF ALL PAIRS OF ALGORITHMS ON F_d VALUE

	LiNGAM	GC	GS	Patel	AIAEC	ACOEC	VACOEC
P-corr	0.046	0.999	0.074	0.315	0.0008	0.0004	6.29×10^{-8}
LiNGAM		0.003	0.999	0.993	0.953	0.856	0.081
GC			0.005	0.046	0.0001	2.88×10^{-6}	1.23×10^{-9}
GS				0.998	0.903	0.074	0.049
Patel					0.538	0.348	0.006
AIAEC						0.999	0.657
ACOEC							0.829

To further compare the statistical differences between these algorithms, we use the Friedman test with post-hoc tests [31] to attest the corresponding algorithms with the confidence level 95%, i.e., the probability of producing the difference by chance is not greater than 5%. If the p-value obtained from the test is less than 0.05, we consider that a significant difference exists in the corresponding experimental results. The result of the Friedman test shows that there is a significant difference between the 8 compared algorithms (p-value = $8.61 \times 10^{-13} < 0.05$). Since significant differences are detected between the compared algorithms by the Friedman test, there are several post-hoc tests that can be applied to find out which algorithms differ from the others. The post-hoc test results of all pairs of algorithms on F_d value are shown in Table IV.

To reduce the chances of obtaining false-positive results when multiple pairwise tests are performed on Table IV, we use the Bonferroni correction to correct for the multiple comparisons [32]. From Table IV, we can find that there are 28 hypotheses simultaneously exist in the multiple comparisons, with a critical p-value of 0.05. In this situation, where p-value $< 0.05/28 = 0.0018$ indicates that the corresponding two algorithms have a statistically significant different effect on the performance and vice versa. We can see the p-values of VACOEC and P-corr, VACOEC and GC are all less than 0.0018, which means VACOEC is significantly different from these methods. Combining these results with the results in Table III, we can come to the conclusion that VACOEC is significantly superior to these algorithms on F_d value, which indicates that VACOEC has better performance on identifying brain effective connectivity.

Finally, we present the time performance of 8 algorithms on each simulated dataset. As is shown in Table V, Patel's running time is the shortest. LiNGAM, AIAEC, ACOEC, and VACOEC are well-matched, whose running times are shorter than P-corr, GC, and GS. In particular, VACOEC's time performance has certain advantages compared with other algorithms, only worse than Patel, and worse than LiNGAM in some simulations. So compared with other algorithms, the computational time over most simulated fMRI data sets of the new algorithm is in the upper middle level. From Table V we also find, the main two factors that affect the algorithms' running time are the number of nodes and the session duration.

Therefore, the VACOEC is better or comparable to the seven comparison algorithms, so we only use it in real fMRI data for new explorations in the following section.

TABLE V
THE TIME PERFORMANCE (RUNNING TIME) OF 8 ALGORITHMS
ON 28 SIMULATIONS

Sim	Algorithms (second)							
	P-corr	LiNGAM	GC	GS	Patel	AIAEC	ACOEC	VACOEC
Sim1	30.54	0.49	0.92	2.07×10^2	0.03	0.69	0.39	0.38
Sim2	58.75	0.85	8.35	9.34×10^2	0.19	2.91	2.27	0.79
Sim3	88.59	1.12	19.32	2.18×10^3	0.61	10.23	9.55	1.88
Sim4	320.55	18.42	309.10	2.53×10^4	4.75	189.75	202.01	33.96
Sim5	156.41	0.63	13.69	7.43×10^3	0.12	21.17	15.53	4.56
Sim6	624.33	0.78	55.26	3.48×10^4	0.53	12.96	10.13	5.48
Sim7	1248.31	1.18	76.03	1.33×10^5	0.60	12.47	10.15	5.10
Sim8	28.72	0.49	2.34	2.11×10^2	0.05	0.56	0.42	0.39
Sim9	1251.45	1.26	76.35	1.33×10^5	0.06	13.43	12.33	12.03
Sim10	29.01	0.48	2.33	2.10×10^2	0.05	5.52	3.98	1.57
Sim11	58.03	0.78	8.16	9.38×10^2	0.20	5.67	4.04	1.56
Sim12	58.09	2.64	8.40	9.33×10^2	0.19	2.895	2.08	0.69
Sim13	28.80	0.47	2.29	2.08×10^2	0.06	0.54	0.38	0.37
Sim14	28.59	0.49	2.42	2.10×10^2	0.06	0.62	0.39	0.37
Sim15	29.09	0.43	2.26	2.07×10^2	0.05	0.56	0.42	0.38
Sim16	28.85	0.40	2.35	2.08×10^2	0.05	0.60	0.39	0.37
Sim17	58.41	0.35	8.21	9.32×10^2	0.21	1.98	2.23	0.93
Sim18	28.82	0.34	2.37	2.08×10^2	0.05	0.51	0.37	0.34
Sim19	697.11	0.77	31.31	3.00×10^4	0.21	0.65	0.58	0.56
Sim20	698.98	0.86	31.30	3.01×10^4	0.23	0.61	0.59	0.57
Sim21(a)	15.10	0.21	1.21	1.10×10^2	0.03	0.11	0.08	0.08
Sim21(b)	14.99	0.23	1.17	1.08×10^2	0.03	0.11	0.08	0.08
Sim22	28.99	0.45	2.23	2.10×10^2	0.05	0.53	0.36	0.35
Sim23	31.83	0.47	2.21	2.09×10^2	0.05	0.58	0.42	0.41
Sim24	29.17	0.48	2.27	2.09×10^2	0.05	0.68	0.47	0.45
Sim25	8.14	0.28	0.91	5.22×10^1	0.02	0.21	0.16	0.16
Sim26	4.40	0.16	0.49	1.31×10^1	0.01	0.10	0.08	0.08
Sim27	4.34	0.15	0.53	1.36×10^1	0.01	0.11	0.09	0.08
Sim28	9.01	0.28	0.86	5.24×10^1	0.03	0.21	0.17	0.16

F. Experiments on the Real fMRI Data

The study was conducted under a research protocol approved by the Institutional Review Board of the Xuanwu Hospital (IRB-2016-004), in accordance with the Declaration of Helsinki. All participants were given a detailed explanation of the study and signed an informed consent prior to the study. As the numbers of both healthy and diseased subjects in our dataset are small, we also use a large-scale dataset called the ADNI database (adni.loni.usc.edu).

1) *Experimental Results on the Collected fMRI Data:* Our collected MRI data were acquired with a 3-Tesla Trio scanner (Siemens, Erlangen, Germany). All participants were asked to hold still, with their eyes closed. Foam padding was employed to limit head motion and headphones were used to reduce scanner noise. Resting-state functional magnetic resonance imaging (rs-fMRI) images were acquired using an echo-planar imaging (EPI) sequence with a repetition time (TR)/echo time (TE)/flip angle (FA) = 2000 ms/40 ms/90°, 28 axial slices, slice thickness/gap = 4/1 mm, field of view (FOV) = 256 mm, bandwidth = 2232 Hz/pixel and number of repetitions = 239. The 3D T1-weighted anatomical image was acquired with a magnetization-prepared rapid gradient echo (MPRAGE) method with the following parameters: TR/TE/inversion time (TI)/FA = 1900 ms/2.2 ms/900 ms/9°, matrix = 256 × 224, bandwidth = 199 mm, 176 sagittal slices with 1 mm thickness. The clinical characteristics of the 13 AD patients and 10 NCs

TABLE VI
THE CLINICAL CHARACTERISTICS OF THE NC AND AD PATIENTS

Characteristics	NC (n=10)	AD (n=13)
Age (years)	61.5±8.4 ¹	69.2±6.2
Gender (male/female)	5/5	8/5
Education (years)	9.4±3.9	10.9±4.1
CDR ²	0	0.5
MoCA ³	25.8±1.2	21.1±2.7

¹Values represent means ± standard deviation.

²CDR: Clinical Dementia Rate.

³MoCA: Montreal Cognitive Assessment.

TABLE VII
THE REGIONS OF INTEREST IN THE REAL fMRI DATA

Network	Number	ROI	Detailed description
DMN ¹	1	PCC	Posterior Cingulate Cortex
	2	LIPL	Left Inferior Parietal Lobe
	3	RIPL	Right Inferior Parietal Lobe
	4	MPFC	Medial Prefrontal Cortex
ECN ²	5	LDLPFC	Left Dorsolateral Prefrontal Cortex
	6	LPCC	Left Posterior Parietal Cortex
	7	RDLPPC	Right Dorsolateral Prefrontal Cortex
	8	RPPC	Right Posterior Parietal Cortex
	9	APFC	Anterior Prefrontal Cortex
SN ³	10	dACC	Dorsal Anterior Cingulate Cortex
	11	RFIC	Right Frontoinsular Cortex
	12	LFIC	Left Frontoinsular Cortex

¹DMN: Default Mode Network.

²ECN: Executive Control Network.

³SN: Salience Network.

are shown in Table VI. fMRI data preprocessing was performed using SPM12 toolbox.¹

In our experiments, we select twelve ROIs that are considered to be potentially relevant to AD based on the literature [33], [34]. These ROIs are defined by the parcellation map from Power *et al.* (2011) [33]. Please see Table VII for the name of each ROI from three networks.

The effective connectivity network of NC and AD identified by VACOEC are shown in Fig. 7. In Fig. 7, the red dotted line divides the entire network into nine regions. In particular, the first region divided by red dotted line shows the effective connectivity in DMN, the second region to its right shows the effective connectivity between the DMN and ECN, and the third region to its right shows the effective connectivity between the DMN and SN. The rest of the regions' meaning are the same as them.

From the result in Fig. 7, we can draw the conclusion: 1) The connection relationship in DMN: Both $LIPL \rightarrow RIPL$ and $LIPL \rightarrow MPFC$ exist in the NC and AD, while the effective connective $MPFC \rightarrow PCC$ is missing in the AD patients' networks. 2) The connection relationship between DMN and ECN: there are six effective connectivity between the DMN and ECN in NC and AD, which means the connections in this network of the AD patients remain to be intact. Moreover, there are some connections in AD patients that are reverse to those in NCs, these reverse connections may have an effect on AD. 3) The connection relationship between DMN and SN: there are three connections in NC which are $dACC \rightarrow PCC$,

¹The toolbox is available at <http://www.fil.ion.ucl.ac.uk/spm>.

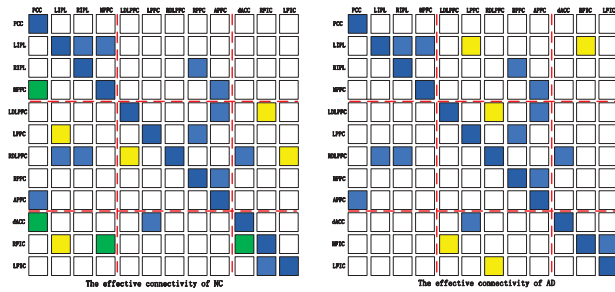


Fig. 7. The effective connectivity learned by VACOEC from fMRI data of NC and AD. The horizontal and vertical coordinates indicate the corresponding regions of interest, the color grid indicates an effective connectivity between the two corresponding regions which is obtained by the VACOEC: the blue grid shows the effective connectivity exists simultaneously in both NC and AD, the yellow grid shows the effective connectivity has the opposite directions in NC and AD, and the green grid shows that the effective connectivity only exists in NC while are missing in AD. The red dotted line divides the entire network into nine regions, including the effective connectivity in the three networks (DMN, ECN and SN) and the effective connectivity between each of two corresponding networks.

$RFIC \rightarrow LIPL$, and $RFIC \rightarrow MPFC$, while there are only one connection $LIPL \rightarrow RFIC$. Two connections are missing in AD patients' network, which may indicate the missing connections between DMN and SN is a factor that causes AD. 4) The connection relationship in ECN: the number of connections in ECN of NC and AD are the same, and there are two connections in AD patients that are reverse to those in NCs. 5) The connection relationship between ECN and SN: the result is similar to 4). 6) The connection relationship in SN: the effective connectivity in SN are different between AD and NC. In NC, there are two connections, $RFIC \rightarrow dACC$ and $LFIC \rightarrow RFIC$, while in AD, there is only one connection, $RFIC \rightarrow LFIC$. Generally, we can see that there are some missing and reversing effective connectivity in the three networks of AD patients compared to NCs. The missing effective connectivity in DMN and SN could be the cause of Alzheimer's disease in the elderly, which has been confirmed by many existing studies [5], [31]. The reversing effective connectivity, which can not be found in functional network studies, may also be a cause of Alzheimer's disease in the elderly. The current study found that there are specific disruptions of the effective connectivity in the DMN of AD patients [34]. These findings are also verified by our results in Fig. 7 that some effective connectivity ($MPDC \rightarrow PCC$, $dACC \rightarrow PCC$, and $RFIC \rightarrow MPFC$) in DMN (or between DMN and other networks) are missing in AD compared with NC. Besides, Dobryakova *et al.* found that the effective connectivity $dACC \rightarrow PCC$ exists in NCs, but it is missing in Primary Progressive Multiple Sclerosis (PPMS) [35]. This finding is exactly consistent with our results in Fig. 7, which indicates that effective connectivity can help us understand the differences between healthy people and people with a disease. [34]–[36] To further explore the performance of VACOEC algorithm in large-scale brain nodes and multiple subjects, we carry out some experiments on another real fMRI dataset below.

2) *Experimental Results on the ADNI Database:* Another real dataset used in this article was obtained from the ADNI

TABLE VIII
THE CLINICAL CHARACTERISTICS OF THE NC, MCI AND AD PATIENTS

Characteristics	NC (n=75)	MCI (n=76)	AD (n=69)
Age (years)	77.6±7.3	71.9±6.2	74.8±7.6
Gender (male/female)	40/35	40/36	28/41

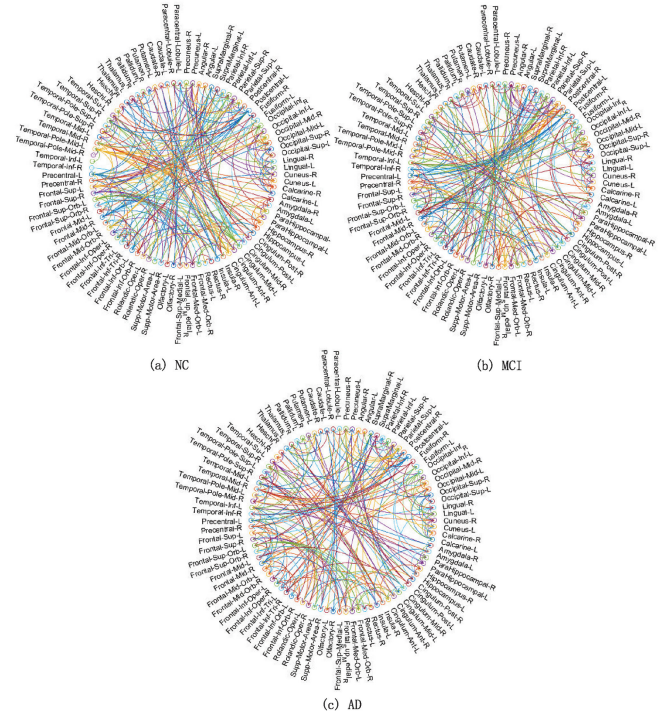


Fig. 8. The effective connectivity learned by VACOEC from ADNI data of NC, MCI and AD groups.

database. To date, over 1500 adults, aged 55 to 100, were recruited to participate in the research, consisting of cognitively normal controls (NC) older individuals, patients with Mild Cognitive Impairment (MCI), and patients with Alzheimer's disease (AD). For more information, see www.adniinfo.org. In this study, a total of 220 subjects of the ADNI database are studied. These subjects belong to 3 groups according to ADNI baseline diagnosis: NCs, MCIs, and AD patients. Demographic data (age and gender) is shown in Table VIII.

The EC networks learned for 3 different groups are graphically rendered in a circular diagram format in Fig. 8, where the outermost rings represent the brain regions and the center is a representation of brain effective connectivity. Each circular diagram is obtained by VACOEC on the corresponding dataset. We employ the Automated Anatomical Labeling (AAL) template as the parcellation map to define the brain regions (contain 90 ROIs). Each brain region is represented by a circle with different colors (some may be same), and the color of arrows are the same with the parent nodes.

Following the chain of NC-MCI-AD in Fig. 8, the number of brain effective connectivity in each group is respectively 334, 302, and 281. In other words, the group of AD has 7.0 percent less amount of effective connectivity than MCI and 15.9 percent less amount of effective connectivity than NC. This

result shows that as the disease worsens, the number of brain effective connectivity will be less and less. Loss of connectivity in AD has been widely reported in the literature [37], [38]. Aside from having different amounts of brain effective connectivity at the global scale, AD may also have a different pattern of connectivity across the brain compared with MCI and NC. Therefore, we count the number of arcs in each of the brain regions to find the different patterns of connectivity between 3 different groups. The results show that there are significant decreases of brain effective connectivity in the brain regions of Cingulum, Precuneus, Insula, and Hippocampus. These findings are also corroborated by previous studies that have implicated changes in these regions to be related with MCI and AD [37]. Previous pathological studies observed that neuropathological hallmarks accumulate in the hippocampus, and found that loss of effective connectivity in the hippocampus is related to AD [5], [38]. Our finding that the number of brain effective connectivity of AD between the hippocampus and other brain regions is decreased further verifies it, which is in agreement with previous studies and can help to explain and predict the progression and evolution of the AD disease [5]. Besides, the cingulum is a major structure of the limbic system, which is closely associated with memory function, and the decreased number of effective connectivity in the cingulum may be a factor causing AD in the elderly. This finding is also consistent with the results in our collected fMRI dataset.

V. CONCLUSION

This paper presents a novel Bayesian network method for learning brain EC network structures from fMRI data, i.e., VA-COEC. The algorithm first uses the voxel activation information to measure the independence between each pair of brain regions, and effectively restricts the space of candidate solutions, which avoids many unnecessary searches by ants. Then, it combines the global score increase of a solution with the voxel activation information, and introduces a new heuristic function with better heuristic ability to enhance the solution quality. The experimental results illustrate that the new algorithm is superior both in terms of quality of the solutions and computational time to other compared algorithms on most simulated fMRI data sets we have tested. Moreover, the results on the real fMRI data show that AD patients experience decreased effective connectivity in some brain regions compared to NC, and as the disease worsens, the number of effective connectivity will be less and less. These findings are corroborated by previous studies that have implicated changes of EC to be related with MCI and AD, which can help to explain and predict the progression and evolution of the AD disease.

REFERENCES

- [1] K. J. Friston, "Functional and effective connectivity in neuroimaging: A synthesis," *Human Brain Mapping*, vol. 2, no. 1, pp. 56–78, 1994.
- [2] B. M. Hampstead, M. Khoshnoodi, W. Yan, G. Deshpande, and K. Sathian, "Patterns of effective connectivity during memory encoding and retrieval differ between patients with mild cognitive impairment and healthy older adults," *NeuroImage*, vol. 124, pp. 997–1008, 2016.
- [3] C. S. Pattichis, C. Pitris, J. Liang, and Y. Zhang, "Guest editorial on the Special Issue on Integrating Informatics and Technology for Precision Medicine," *IEEE J. Biomed. Health Inform.*, vol. 23, no. 1, pp. 12–13, Jan. 2019.
- [4] R. Rytzar, E. Fornari, R. S. Frackowiak R S, J. A. Ghika, and M. G. Knyazeva, "Inhibition in early Alzheimer's disease: An fMRI-based study of effective connectivity," *NeuroImage*, vol. 57, no. 3, pp. 1131–1139, 2011.
- [5] Y. Zhong, L. Huang, S. Cai, K. M. V. Deneen, A. Ren, and J. Ren, "Altered effective connectivity patterns of the default mode network in Alzheimers disease: An fMRI study," *Neurosci. Lett.*, vol. 578, pp. 171–175, 2014.
- [6] H. Cagnan, E. P. Duff, and P. Brown, "The relative phases of basal ganglia activities dynamically shape effective connectivity in Parkinson's disease," *Brain*, vol. 138, no. 6, pp. 1667–1678, 2015.
- [7] B. Mohl, B. D. Berman, E. Shelton, and J. Tanabe, "Levodopa response differs in Parkinsons motor subtypes: A task-based effective connectivity study," *J. Comparative Neurol.*, vol. 525, no. 9, pp. 2192–2201, 2017.
- [8] J. Cai, A. Liu, T. Mi, S. Garg, W. Trappe, M. J. McKeown, and Z. J. Wang, "Dynamic graph theoretical analysis of functional connectivity in Parkinson's disease: The importance of fiedler value," *IEEE J. Biomed. Health Inform.*, vol. 23, no. 4, pp. 1720–1729, Jul. 2019.
- [9] N. L. Hutcheson, K. R. Sreenivasan, G. Deshpande, M. A. Reid, and J. Hadley, "Effective connectivity during episodic memory retrieval in schizophrenia participants before and after antipsychotic medication," *Human Brain Mapping*, vol. 36, no. 4, pp. 1442–1457, 2015.
- [10] D. Mastrovito, C. Hanson, and S. J. Hanson, "Differences in atypical resting-state effective connectivity distinguish autism from schizophrenia," *NeuroImage Clin.*, vol. 18, pp. 367–376, 2018.
- [11] J. Dauwels, F. Vialatte, T. Musha, and A. Cichocki, "A comparative study of synchrony measures for the early diagnosis of Alzheimers disease based on EEG," *NeuroImage*, vol. 49, no. 1, pp. 668–693, 2010.
- [12] Y. Wang, O. David, X. Hu, and G. Deshpande, "Can Patels accurately estimate directionality of connections in brain networks from fMRI?" *Magn. Reson. Med.*, vol. 78, no. 5, pp. 2003–2010, 2017.
- [13] R. S. Patel, F. D. B. Bowman, and J. K. Rilling, "A Bayesian approach to determining connectivity of the human brain," *Human Brain Mapping*, vol. 27, no. 3, pp. 267–276, 2006.
- [14] S. Shimizu, P. O. Hoyer, A. Hyvärinen, and A. Kerminen, "A linear non-Gaussian acyclic model for causal discovery," *J. Mach. Learn. Res.* vol. 7, pp. 2003–2030, 2006.
- [15] L. Xu, T. Fan, X. Wu, K. Chen, and X. Guo, "A pooling-LiNGAM algorithm for effective connectivity analysis of fMRI data," *Frontiers Comput. Neurosci.*, vol. 8, no. 8, 2014, Art. no. 125.
- [16] A. K. Seth, "A MATLAB toolbox for Granger causal connectivity analysis," *J. Neurosci. Methods*, vol. 186, no. 2, pp. 262–273, 2010.
- [17] W. Liao, D. Marinazzo, Z. Pan, Q. Gong, and H. Chen, "Kernel Granger causality mapping effective connectivity on FMRI data," *IEEE Trans. Med. Imag.*, vol. 28, no. 11, pp. 1825–1835, Nov. 2009.
- [18] N. Frolov, V. Maksimenko, A. Lüttjohann, A. Koronovskii, and A. Hramov, "Feed-forward artificial neural network provides data-driven inference of functional connectivity," *Chaos*, vol. 29, Nov. 2019, Art no. 091101.
- [19] N. Xu, R. N. Spreng, and P. C. Doerschuk, "Initial validation for the estimation of resting-state fMRI effective connectivity by a generalization of the correlation approach," *Frontiers Neurosci.*, vol. 11, 2017, Art. no. 271.
- [20] G. Niso *et al.*, "HERMES: Towards an integrated toolbox to characterize functional and effective brain connectivity," *Neuroinform.*, vol. 11, no. 4, pp. 405–434, 2013.
- [21] A. M. Bastos and J. M. Schoffelen, "A tutorial review of functional connectivity analysis methods and their interpretational pitfalls," *Frontiers Syst. Neurosci.*, vol. 9, 2016, Art. no. 175.
- [22] S. M. Smith *et al.*, "Network modelling methods for FMRI," *NeuroImage*, vol. 54, no. 2, pp. 875–891, 2011.
- [23] K. J. Friston, A. M. Bastos, A. Oswal, B. Wijk, C. Richter, and V. Litvak, "Granger causality revisited," *NeuroImage*, vol. 101, pp. 796–808, 2014.
- [24] L. Zhou, L. Wang, L. Liu, P. Ogunbona, and D. Shen, "Learning discriminative Bayesian networks from high-dimensional continuous neuroimaging data," *IEEE Trans. Pattern Anal. Mach. Intell.*, vol. 38, no. 11, pp. 2269–2283, Nov. 2016.
- [25] J. Ji, J. Liu, P. Liang, and A. Zhang, "Learning effective connectivity network structure from fMRI data based on artificial immune algorithm," *Plos One*, vol. 11, no. 4, 2016, Art. no. e0152600.
- [26] J. Liu, J. Ji, A. Zhang, and P. Liang, "An ant colony optimization algorithm for learning brain effective connectivity network from fMRI data," in *Proc. IEEE Int. Conf. Bioinf. Biomed.*, 2016, pp. 360–367.

- [27] L. M. D. Campos, J. M. Fernández-Luna, J. A. Gmez, and J. M. Puerta, "Ant colony optimization for learning Bayesian networks," *Int. J. Approx. Reasoning*, vol. 31, no. 3, pp. 291–311, 2002.
- [28] W. Xue, D. B. Bowman, A. V. Pileggi, and A. R. Mayer, "A multimodal approach for determining brain networks by jointly modeling functional and structural connectivity," *Frontiers Comput.*, vol. 9, 2015, Art. no. 22.
- [29] J. Ji, H. Zhang, R. Hu, and C. Liu, "A Bayesian network learning algorithm based on independence test and ant colony optimization," *Acta Automatica Sinica*, vol. 35, no. 2, pp. 281–288, 2009.
- [30] E. S. Adabor, G. K. Acquaaah-Mensah, and F. T. Oduro, "SAGA: A hybrid search algorithm for Bayesian network structure learning of transcriptional regulatory networks," *J. Biomed. Informat.*, vol. 53, pp. 27–35, 2015.
- [31] D. G. Pereira, A. Afonso, and F. M. Medeiros, "Overview of Friedmans test and post-hoc analysis," *Commun. Statist.-Simul. Comput.*, vol. 44, no. 10, pp. 2636–2653, 2015.
- [32] J. M. Bland and D. G. Altman, "Multiple significance tests: The Bonferroni method," *BMJ*, vol. 310, no. 6973, 1995, Art. no. 170.
- [33] J. D. Power *et al.*, "Functional network organization of the human brain," *Neuron*, vol. 72, no. 4, pp. 665–678, 2011.
- [34] M. Scherr *et al.*, "Effective connectivity in the default mode network is distinctively disrupted in Alzheimer's disease—A simultaneous resting-state FDG-PET/fMRI study," *Human Brain Mapping*, 2019. [Online]. Available: <https://onlinelibrary.wiley.com/doi/pdf/10.1002/hbm.24517>
- [35] E. Dobryakova, M. A. Rocca, P. Valsasina, J. DeLuca, and M. Filippi, "Altered neural mechanisms of cognitive control in patients with primary progressive multiple sclerosis: An effective connectivity study," *Human Brain Mapping*, vol. 38, no. 8, pp. 2580–2588, 2017.
- [36] S. F. Storti, I. B. Galazzo, S. Khan, P. Manganotti, and G. Menegaz, "Exploring the epileptic brain network using time-variant effective connectivity and graph theory," *IEEE J. Biomed. Health Informat.*, vol. 21, no. 5, pp. 1411–1421, Sep. 2017.
- [37] S. Huang *et al.*, "A sparse structure learning algorithm for Gaussian Bayesian network identification from high-dimensional data," *IEEE Trans. Pattern Anal. Mach. Intell.*, vol. 35, no. 6, pp. 1328–1342, Jun. 2013.
- [38] S. Afshari and M. Jalili, "Directed functional networks in Alzheimer's disease: Disruption of global and local connectivity measures," *IEEE J. Biomed. Health Informat.*, vol. 21, no. 4, pp. 949–955, Jul. 2017.